

Journal of Materials Chemistry A

Accepted Manuscript



This is an *Accepted Manuscript*, which has been through the Royal Society of Chemistry peer review process and has been accepted for publication.

Accepted Manuscripts are published online shortly after acceptance, before technical editing, formatting and proof reading. Using this free service, authors can make their results available to the community, in citable form, before we publish the edited article. We will replace this *Accepted Manuscript* with the edited and formatted *Advance Article* as soon as it is available.

You can find more information about *Accepted Manuscripts* in the [Information for Authors](#).

Please note that technical editing may introduce minor changes to the text and/or graphics, which may alter content. The journal's standard [Terms & Conditions](#) and the [Ethical guidelines](#) still apply. In no event shall the Royal Society of Chemistry be held responsible for any errors or omissions in this *Accepted Manuscript* or any consequences arising from the use of any information it contains.

Low-temperature, solution processed metal sulfide as electron transport layer for efficient planar perovskite solar cells

Jiang Liu,^{*,a} Cheng Gao,^{a,b} Lizhu Luo,^c Qinyan Ye,^a Xulin He,^a Liangqi Ouyang,^d Xiaowei Guo,^b
5 Daming Zhuang,^d Cheng Liao,^{*,a} Jun Mei,^a Woonming Lau^a

^a Chengdu Green Energy and Green Manufacturing Technology R&D Centre, Chengdu Development Center of Science and Technology, China Academy of Engineering Physics, Chengdu, 610207, China

^b School of Optoelectronic Information, University of Electronic Science and Technology, Chengdu,
10 610054, China

^c Science and Technology and Surface Physics and Chemistry Laboratory, 71835, Mianyang, 621907, Sichuan, China.

^d School of Materials Science and Engineering, Tsinghua University, Beijing, China.

15 * Corresponding author

E-mail address: 546jiang@163.com (J. Liu); cliao315@hotmail.com (C. Liao)

Abstract

20 Organic-inorganic halide perovskites possess excellent chemical, optical, and electronic properties that make them attractive for next-generation solar cells. In this paper, we introduce all-low-temperature processed perovskite solar cells using metal sulfide as electron transport layer. First, we evaluated the alignment of energy levels at the perovskite/metal sulfide layer interface. The properties of metal sulfide and perovskite layer, as well as the corresponding device performance, were then investigated.
25 Using CdS layer as electron transport layer, we have achieved a maximum power conversion efficiency of 11.2% under reverse scans. The successful use of CdS layer into perovskite solar cells likely would create new pathways and opportunities for the advancement of device design.

Introduction

The last two years have seen an unprecedented growth of interest in organic-inorganic halide
30 perovskite based solar cells due to its distinct combination of high efficiency and easy preparation. Impressive progress in improving the photovoltaic performance has been made in this field. In 2009, Kojima *et al*¹ first reported the use of lead halide perovskites as photosensitizers in liquid-type sensitized TiO₂ solar cells and achieved a power conversion efficiency (PCE) of 3.8%. However, those liquid-type perovskite solar cells encountered serious problems of durability and stability.¹⁻³
35 All-solid-state perovskite solar cells were then developed to achieve good stability and high efficiency using spiro-OMeTAD as a hole transporting material.^{4,5} Many literatures⁶⁻⁸ have also confirmed that under normal photovoltaic operating conditions perovskite solar cells are not excitonic style solar cells, differing from some organic photovoltaic devices in which photogenerated species are strongly bound and can't spontaneously dissociate into free carriers. This means that perovskite solar cells are comparable to inorganic solar cells and may reach above 20% efficiency⁹ with addition of the features
40 of ambipolar charge transport¹⁰ and long electron-hole diffusion length^{11,12}. Until now, an increasing number of research groups have demonstrated perovskite-based solar cells with efficiencies >15%.⁸

13-18

Mesoscopic and planar perovskite-based solar cells both have shown a very promising photovoltaic performance. Evolving from dye-sensitized solar cells, initially a metal-oxide scaffold is always employed in perovskite solar cells. Since the pioneering work of Liu *et al*¹⁹, who demonstrated a simple planar heterojunction solar cell with efficiency of over 15%, planar perovskite devices have been receiving great attention due to the simplicity in processing. Although the perovskite layers could be prepared at a relatively low temperature (around 100 °C),²⁰ most of these high efficient perovskite solar cells typically have employed high-temperature (> 450 °C) processed TiO₂ as electron transport layer, which significantly limits the application of perovskite solar cells in a broader range of substrate. Lots of efforts have been done to produce all-low-temperature perovskite solar cells. Snaith's group^{21, 22} have developed low-temperature processed anatase TiO₂ nanoparticles and achieved a maximum power conversion of over 15%. Inverted planar perovskite solar cells with organic charge material PCBM ((6,6)-phenyl-C61-butyric acid methyl ester) have also been developed to obtain low-temperature processing condition.²³⁻²⁵ In addition, many groups have demonstrated low-temperature processed n-type semiconductors (ZnO^{17, 26}, CdSe²⁷) as electron conductor in perovskite solar cells. Such a simple substitution for TiO₂ layer also results in improvements to device performance, greatly showing the potential for other similar alternative materials.

In this manuscript, we introduced all-low-temperature TiO₂-free planar perovskite solar cells, in which n-type TiO₂ is replaced with metal sulfide (CdS, ZnS) as electron transport layer. These metal sulfides have achieved success in the application as buffer-layer materials to CIGS or CdTe solar cells, due to their good optical and electrical properties.^{28, 29} Further, they can be deposited through solution process at low temperature, making it compatible with flexible substrates. The feasibility of the perovskite solar cells with metal sulfide layer was first evaluated using photoemission spectroscopy. The characterization of device performance was carried out under both forward and reverse scans. By applying solution processed CdS as electron selective layer, the perovskite solar cells with ITO/CdS/perovskite/spiro-OMeTAD/Au planar structures delivers a maximum power conversion efficiency of 11.2% under reverse scans. Our results show the application possibility of more inorganic semiconductor materials, akin to CdS, in perovskite-based solar cells, and also provide principle for the choice of electron transport layer to efficient perovskite solar cells.

Results and discussion

The device structure used in this study is shown in Fig. 1a. In this configuration, a thin ZnS or CdS film was first deposited on tin-doped indium oxide (ITO) glass by chemical bath deposition (CBD),^{29, 30} and then CH₃NH₃PbI₃ light harvester was deposited through a solvent washing process.¹³ The details of the experimental methods are described in the supplementary information. After a short-time thermal annealing, an organic hole transport layer spiro-OMeTAD and gold contact electrode were sequentially deposited on the top of perovskite layer to complete solar cells with ITO/CdS(or ZnS)/perovskite/spiro-OMeTAD/Au planar structure.

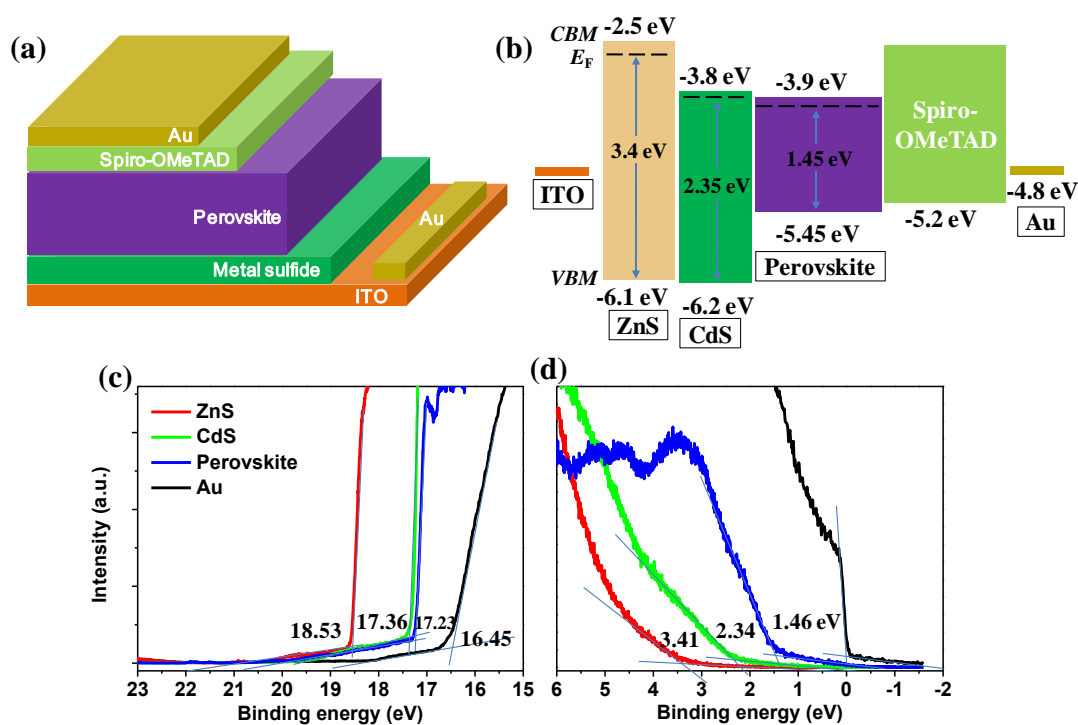


Fig.1. (a) Device structure of the planar perovskite solar cells fabricated in this work. (b) The energy diagram of each layer. (c, d) Ultraviolet photoelectron spectra of ZnS, CdS, perovskite films and gold.

To gain insight into the interface properties of the solar cells used in this study, ultraviolet photoelectron spectra (UPS) were obtained to determine the band offset at CdS (or ZnS)/perovskite hetero-interface, as shown in Fig.1(c d). Obvious difference can be observed between these films. The data are presented as photoemission intensity versus binding energy. The binding energy cutoff in the range of 15-20 eV (Fig.1c) can be used to obtain the work function by subtracting the energy from the He I photon energy (21.22 eV), while the low binding energy onset region (Fig.1d) in the range of 0-6 eV can be used to calculate the valence bands relative to Fermi level. In order to eliminate the possible instrumental bias during data acquisition, the spectra from a sputter-etched gold (Au) was used for reference. Determining the binding energy shift between Au and the films under test yields the valence band maximum (VBM) positions (relative to Fermi level) to be 1.46 eV for $\text{CH}_3\text{NH}_3\text{PbI}_3$ layer, 2.34 eV for CdS and 3.41 eV for ZnS film. Taking into account the reported band gap^{5, 31, 32} for these films (1.55 eV for $\text{CH}_3\text{NH}_3\text{PbI}_3$, 2.4 eV for CdS and 3.6 eV for ZnS film), the energy band diagram is summarized in Fig.1b. Obviously, the prepared CdS and ZnS films, as well as the perovskite film, exhibit as n-type semiconductors with Fermi level closer to the conduction band than to the valence band, consistent with previous work³³. The obtained conduction band energy (relative to vacuum level) for perovskite layer is approximately 3.9 eV, which is also in good agreement with previously reported results⁴. The conduction band offset (CBO) between the perovskite and electron transport layer (ETL) may strongly influence the electron injection across the interface. From the Fig.1b, the CBO at CdS/perovskite interface was determined to be -0.1 eV, while that was +1.3 eV at ZnS/perovskite interface. This led us to predict that CdS may behave better as electron transport layer than ZnS.

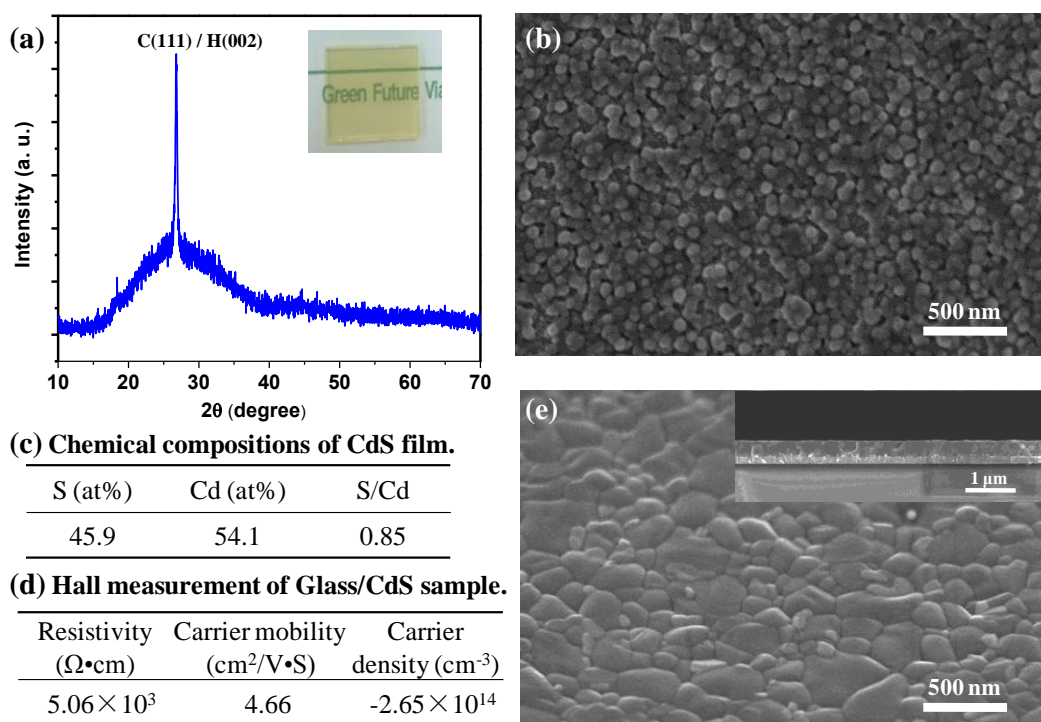


Fig.2. (a) XRD spectra of CdS film on glass substrate (inset shows a photograph of the CdS-coated sample). (b) Surface SEM images of CdS film on ITO-coated substrate. (c) Chemical compositions (measured by XRF) of CdS film. (d) Hall effect measurement result of CdS film on glass substrate. (e) Tilt surface SEM images of perovskite film grown on the ITO/CdS substrate (inset shows the cross-section SEM images of the sample).

Fig.2a shows the XRD spectra of CdS film on glass substrate. Only one weak peak at $2\theta = 27^\circ$ could be found, which may be attributed to CdS cubic structure (111) or hexagonal structure (002). Fig.2b shows the SEM surface morphology of CdS film. We can find that the grain size was very uniform and the substrate was completely covered by CdS film, which also could act as a compact layer to prevent leakage current. XRF measurement (Fig.2c) shows that the prepared CdS film exhibits an S/Cd atomic ratio of 0.85, which can be explained the presence of CdO. Hall-effect measurement (Fig.2d) further confirms that the prepared CdS film is an n-type semiconductor, where carrier mobility and concentration are $4.66 \text{ cm}^2/\text{V} \cdot \text{S}$ and $-2.65 \times 10^{14} \text{ cm}^{-3}$, respectively. Obtaining uniform, pinhole-free perovskite films on planar substrate is important for achieving high-performance devices. In this study, we adopted the solvent-engineering process described in a study of Jeon et al.¹³, in which non-polar solvent (toluene) was dripped on the substrate during spinning to improve film morphology. In order to obtain 300-400 nm thickness perovskite layer, 1.2 M $\text{CH}_3\text{NH}_3\text{I}$ and PbI_2 precursor solution was adopted for spin coating at 3000 rpm after multiple trials (Fig.S2). A typical surface SEM image of perovskite film grown on the ITO/CdS substrate is shown in Fig.2e. We can find that the perovskite film has a dense-microstructure with grain sizes in the range of 100-300 nm and shows a 100% coverage, together with an extremely flat surface. Fig.3a shows the cross-sectional SEM image of a finished device with CdS as electron transport layer. Each layer could be clearly defined according to the contrast variation of the cross-sectional image. The addition of hole transport layer (Spiro-OMeTAD) can also completely coat the perovskite film.

Table 1. Photovoltaic parameters of devices fabricated in this study. The average values were given in

brackets from 10–15 cells for each type of devices

Device	V_{oc} (V)	J_{sc} (mA/cm ²)	FF (%)	PCE (%)
ITO	1.08 (0.97)	7.05 (4.23)	0.47 (0.36)	3.58 (1.54±0.88)
ITO/ZnS	0.98 (0.76)	2.25 (1.73)	0.44 (0.28)	0.98 (0.53±0.37)
ITO/CdS(30nm)	1.05 (1.02)	16.14 (15.58)	0.66 (0.58)	11.17 (9.24±1.48)
ITO/CdS(50nm)	1.01 (1.05)	16.78 (15.05)	0.65 (0.60)	11.00 (9.55±1.07)
ITO/CdS(100nm)	0.96 (0.87)	13.93 (11.32)	0.63 (0.47)	8.52 (5.16±3.24)
FTO/TiO ₂	0.99 (0.95)	17.95 (16.76)	0.72 (0.67)	12.80 (10.35±1.75)

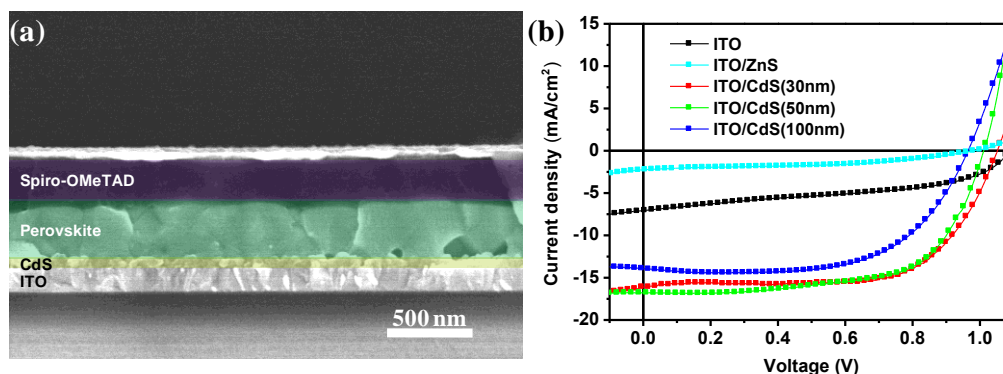


Fig. 3. (a) Cross-sectional SEM image of a completed ITO/CdS(50nm)/CH₃NH₃PbI₃/spiro-OMeTAD/Au planar solar. (b) J-V curves of planar perovskite solar cells with different device structures.

In order to probe the effect of metal sulfide on device performance, perovskite solar cells with and without electron transport layer were fabricated. Fig.3b shows the current density-voltage (J - V) curves for these cells. The photovoltaic parameters are also summarized in Table 1. The device without electron transport layer presents an open circuit voltage (V_{oc}) of 1.08 V, a short circuit current density (J_{sc}) of 7.05 mA/cm² and a fill factor (FF) of 0.47, corresponding to a power conversion efficiency (PCE) of 3.58%. The V_{oc} is remarkable high, but the J_{sc} and FF are very low, which could be attributed to the inefficiency electron transport arising from the spike band alignment at ITO/perovskite interface. The combination of all these parameters only yields a very low efficiency. When ZnS was used as electron transport layer, the device shows an even lower PCE of 0.98% with a V_{oc} of 0.98 V, a J_{sc} of 2.25 mA/cm² and a FF of 0.44. This is primarily due to the large conduction band offset between ZnS and perovskite layer (Fig.1), together with the low crystallinity and high surface roughness of ZnS layer (Fig.S4). Therefore, the addition of ZnS layer would not improve the charge transport, and instead introduce an increased contact resistance. In contrast, devices with CdS layers show a good performance. To obtain the optimal CdS layer, varied CdS film thickness was performed on ITO by controlling the deposition condition (Fig.S5). When a thin CdS layer of about 30 nm was used, a V_{oc} of 1.05 V, a J_{sc} of 16.14 mA/cm² and a FF of 0.66 were achieved, resulting in the champion PCE of 11.17%. The devices with approximately 50 nm thickness CdS layer resulted in very similar results. As the CdS layer thickness is further increased to about 100 nm, the device performance exhibits obvious loss in J_{sc} and FF . Typically, thicker CdS layer results in more absorption loss, thus the reduced J_{sc} . The FF is also largely affected by the series resistance effects from large CdS thickness. Therefore, further increase of CdS thickness would not show improvement in device performance. The

common TiO₂-based planar devices were also fabricated in our lab to compare with CdS-based devices. The champion TiO₂-based solar cell exhibited a power conversion efficiency of 12.8% compared to 11.2% for the champion CdS-based device. Although that, we believe the use of CdS is advantageous in providing a simple low-temperature preparation process. Besides, we compare the hysteresis of perovskite devices with CdS and TiO₂. Typical J-V curves under forward and reverse scan directions for the two kinds of perovskite devices are shown in Figure S6. This CdS-based perovskite solar cell exhibits a little hysteresis of photocurrent, although it is not more serious compared to the TiO₂-based planar perovskite solar cells.

The high charge carrier mobility of the perovskite, along with right charge conductor, can allow for the generation of high voltages³⁴. From the table 1, it also appears surprising that V_{oc} is not affected by lack of the electron transport layer. We surmise that the perovskite layer could behave as a n-type semiconductor and the built-in electric field (or the voltage) is mainly produced at the perovskite/spiro-OMeTAD interface. The high coverage of the perovskite layer further minimizes the voltage loss. In order to better understand the performance differences between with and without CdS layer, electrochemical impedance spectroscopy (EIS) was used to compare their charge transport properties. The obtained spectra (Fig.4) for both samples exhibit obvious differences. According to the previous report³⁵, the lower frequency arc of the impedance spectra is commonly attributed to the recombination resistance (R_{rec}) and R_{rec} is inversely related to the recombination rate. Obviously, the recombination at low bias (<0.8 V) for the CdS/Perovskite/spiro-OMeTAD based devices is lower compared to CdS-free based device. In addition, the R_{rec} in the device with CdS layer decreases slowly until the applied bias voltage (V_{app}) reached 0.7 V. However, for CdS-free device the variation with V_{app} goes gently, even increase slightly at low V_{app} and then declined slightly at high V_{app} . This phenomenon could be explained that the device without electron transport layer is deviated from the common diode model. Very recently, Liu *et al.*³⁶ reported that a compact layer free perovskite solar cell can also yield a PCE of up to 13.5% using two-step solution processed perovskite layer. However, our devices without electron transport layer here behave badly, which may be explained by the differences of perovskite preparation process or charge separation interfaces without residual unreacted PbI₂.

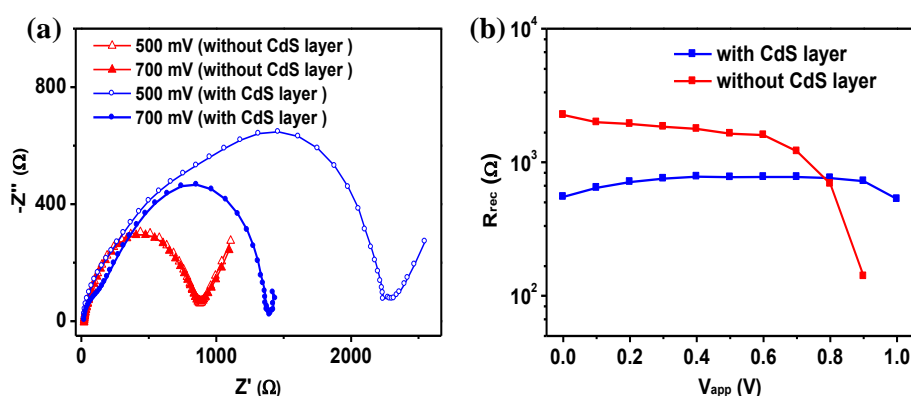


Fig.4. (a) Nyquist plots obtained from the EIS measurement of planar devices with and without electron transport layer. (b) Recombination resistance extracted from the arc at lower frequencies.

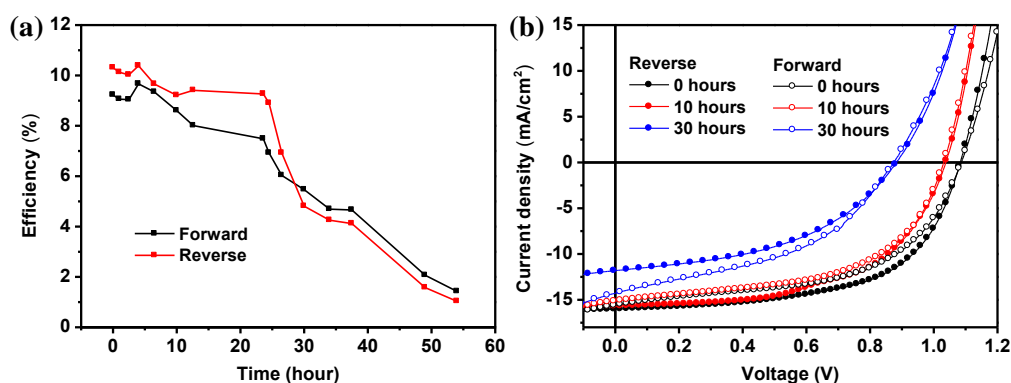


Fig.5. (a) The power conversion efficiency of a well-behaved CdS-based perovskite solar cell as a function of storage time in air. (b) J-V curves of the perovskite solar cell after storage in air for different times.

5

To investigate the air-stability and photocurrent hysteresis in this kind of device, we have also characterized the device performance of a unencapsulated perovskite solar cell as a function of storage time in ambient air (30-40% relative humidity and 20-25 °C temperature) under forward (-0.2 V \rightarrow 1.2 V) and reverse (1.2 V \rightarrow -0.2 V) scans, as shown in Fig.5. The device exhibits a little increased power conversion efficiency during the initial storage time, which could be attributed to the conductivity variation (p-doping) of spiro-OMeTAD layer from the oxidation (exposure in air).^{37,38} The perovskite solar cell exhibits 50% degradation of *PCE* after 24 hours. The degradation rate is very close to the reported result for compact layer free perovskite solar cells.³⁶ This may indicate the CdS is not the dominant factor affecting the air-stability. The *PCE* under reverse scans is 0.4-1.7% higher than that under forward scans during short (< 12 hours) storage time, but then turns lower after over 30 hours storage time.

Conclusion

In summary, we have demonstrated the use of metal sulfide by solution-process deposition as electron transport layer in planar perovskite solar cells. The kind of device allows relatively low temperature processing. The conduction band offset at the interface between perovskite and electron transport layer was found to be very important to reduce energy loss for charge transportation and collection. The photovoltaic performance and impedance spectroscopy reveal the presence of CdS layer results in efficient collection and reduced recombination. We believe that the successful use of solution processed CdS film in perovskite-based solar cells likely extends to more analogous inorganic semiconductor materials, including those n-type semiconductors (CdSe, ZnSe, In₂S₃) which could be used as electron selective layer, as well as those p-type semiconductors (CuInSe₂, CdTe) used as hole selective layer.

Acknowledgements

This work is supported by the National Nature Science Foundation of China (51202227), the Science and Technology Development Foundation of China academy of Engineering Physics (2014A0302015 and 2014B0302054), the National High Technology Research and Development Program of China (2012AA050704), Sichuan International Cooperation Research Project (No. 2014HH0068) and the Fundamental Research Funds for the Central Universities of China (No.2672012ZYGX2012J065).

Notes and references

1. A. Kojima, K. Teshima, Y. Shirai and T. Miyasaka, *Journal of the American Chemical Society*, 2009, **131**, 6050-6051.
- 5 2. J. H. Im, C. R. Lee, J. W. Lee, S. W. Park and N. G. Park, *Nanoscale*, 2011, **3**, 4088-4093.
3. J. H. Im, J. Chung, S. J. Kim and N. G. Park, *Nanoscale research letters*, 2012, **7**, 353.
4. H. S. Kim, C. R. Lee, J. H. Im, K. B. Lee, T. Moehl, A. Marchioro, S. J. Moon, R. Humphry-Baker, J. H. Yum, J. E. Moser, M. Gratzel and N. G. Park, *Scientific reports*, 2012, **2**, 591.
5. M. M. Lee, J. Teuscher, T. Miyasaka, T. N. Murakami and H. J. Snaith, *Science*, 2012, **338**, 643-647.
- 10 6. V. D'Innocenzo, G. Grancini, M. J. Alcocer, A. R. Kandada, S. D. Stranks, M. M. Lee, G. Lanzani, H. J. Snaith and A. Petrozza, *Nat Commun*, 2014, **5**, 3586.
7. J. S. Manser and P. V. Kamat, *Nature Photonics*, 2014, **8**, 737-743.
8. Q. Lin, A. Armin, R. C. R. Nagiri, P. L. Burn and P. Meredith, *Nature Photonics*, 2015, **9**, 106-112.
9. R. F. Service, *Science*, 2014, **344**, 458-458.
- 15 10. W. A. Laban and L. Etgar, *Energy & Environmental Science*, 2013, **6**, 3249.
11. S. D. Stranks, G. E. Eperon, G. Grancini, C. Menelaou, M. J. Alcocer, T. Leijtens, L. M. Herz, A. Petrozza and H. J. Snaith, *Science*, 2013, **342**, 341-344.
12. G. Xing, N. Mathews, S. Sun, S. S. Lim, Y. M. Lam, M. Gratzel, S. Mhaisalkar and T. C. Sum, *Science*, 2013, **342**, 344-347.
- 20 13. N. J. Jeon, J. H. Noh, Y. C. Kim, W. S. Yang, S. Ry and S. I. Seok, *Nature materials*, 2014, **13**, 897-903.
14. J.-H. Im, I.-H. Jang, N. Pellet, M. Grätzel and N.-G. Park, *Nature Nanotechnology*, 2014, **9**, 927-932.
15. H. Zhou, Q. Chen, G. Li, S. Luo, T. B. Song, H. S. Duan, Z. Hong, J. You, Y. Liu and Y. Yang, *Science*, 2014, **345**, 542-546.
16. Q. Xue, Z. Hu, J. Liu, J. Lin, C. Sun, Z. Chen, C. Duan, J. Wang, C. Liao, W. M. Lau, F. Huang, H.-L. Yip and Y. Cao, *Journal of Materials Chemistry A*, 2014, **2**, 19598-19603.
- 25 17. D. Liu and T. L. Kelly, *Nature Photonics*, 2014, **8**, 133-138.
18. Z. Xiao, C. Bi, Y. Shao, Q. Dong, Q. Wang, Y. Yuan, C. Wang, Y. Gao and J. Huang, *Energy & Environmental Science*, 2014, **7**, 2619.
19. M. Liu, M. B. Johnston and H. J. Snaith, *Nature*, 2013, **501**, 395-398.
- 30 20. A. Dualeh, N. Tétreault, T. Moehl, P. Gao, M. K. Nazeeruddin and M. Grätzel, *Advanced Functional Materials*, 2014, **24**, 3250-3258.
21. J. T.-W. Wang, J. M. Ball, E. M. Barea, A. Abate, J. A. Alexander-Webber, J. Huang, M. Saliba, I. Mora-Sero, J. Bisquert, H. J. Snaith and R. J. Nicholas, *Nano letters*, 2014, **14**, 724-730.
22. K. Wojciechowski, M. Saliba, T. Leijtens, A. Abate and H. J. Snaith, *Energy & Environmental Science*, 2014, **7**, 1142.
- 35 23. J. You, Z. Hong, Y. M. Yang, Q. Chen, M. Cai, T.-B. Song, C.-C. Chen, S. Lu, Y. Liu, H. Zhou and Y. Yang, *ACS Nano*, 2014, **8**, 1674-1680.
24. P. Docampo, J. M. Ball, M. Darwich, G. E. Eperon and H. J. Snaith, *Nat Commun*, 2013, **4**, 2761.
25. O. Malinkiewicz, A. Yella, Y. H. Lee, G. M. Espallargas, M. Graetzel, M. K. Nazeeruddin and H. J. Bolink, *Nature Photonics*, 2014, **8**, 128-132.
- 40 26. M. H. Kumar, N. Yantara, S. Dharani, M. Graetzel, S. Mhaisalkar, P. P. Boix and N. Mathews, *Chem Commun (Camb)*, 2013, **49**, 11089-11091.
27. L. Wang, W. Fu, Z. Gu, C. Fan, X. Yang, H. Li and H. Chen, *J. Mater. Chem. C*, 2014, **2**, 9087.
28. J. Liu, D. Zhuang, H. Luan, M. Cao, M. Xie and X. Li, *Progress in Natural Science: Materials International*, 2013, **23**, 133-138.
- 45 29. J. Liu, D.-m. Zhuang, M.-j. Cao, X.-l. Li, M. Xie and D.-w. Xu, *Vacuum*, 2014, **102**, 26-30.

30. L. Larina, D. H. Shin, N. Tsvetkov and B. T. Ahn, *Journal of The Electrochemical Society*, 2009, **156**, D469.
31. Z. Li, J. Wei, P. Li, L. Zhang, E. Shi, C. Ji, J. Liu, D. Zhuang, Z. Liu, J. Zhou, Y. Shang, Y. Li, K. Wang, H. Zhu, D. Wu and A. Cao, *Nano Research*, 2012, **5**, 595-604.
32. L. Larina, D. Shin, J. H. Kim and B. T. Ahn, *Energy & Environmental Science*, 2011, **4**, 3487.
- 5 33. B. Conings, L. Baeten, C. De Dobbelaere, J. D'Haen, J. Manca and H. G. Boyen, *Advanced materials*, 2014, **26**, 2041-2046.
34. E. Edri, S. Kirmayer, D. Cahen and G. Hodes, *The Journal of Physical Chemistry Letters*, 2013, **4**, 897-902.
35. J. A. Christians, R. C. Fung and P. V. Kamat, *Journal of the American Chemical Society*, 2014, **136**, 758-764.
36. D. Liu, J. Yang and T. L. Kelly, *Journal of the American Chemical Society*, 2014, **136**, 17116-17122.
- 10 37. A. Abate, T. Leijtens, S. Pathak, J. Teuscher, R. Avolio, M. E. Errico, J. Kirkpatrick, J. M. Ball, P. Docampo, I. McPherson and H. J. Snaith, *Physical chemistry chemical physics : PCCP*, 2013, **15**, 2572-2579.
38. J. Liu, Y. Wu, C. Qin, X. Yang, T. Yasuda, A. Islam, K. Zhang, W. Peng, W. Chen and L. Han, *Energy & Environmental Science*, 2014, **7**, 2963.

15